J Appl Electrochem (2010) 40:2193–2202
DOI 10.1007/s10800-010-0187-6

ORIGINAL PAPER

A new class of Sol–gel derived $LiM_{1x}M_{2y}Mn_{2-x-y}O_{3.8}F_{0.2}$ (M_1 = Cr, M_2 = V; x = y = 0.2) cathodes for lithium batteries

N. Jayaprakash · N. Kalaiselvi · C. H. Doh · Gangulibabu · D. Bhuvaneswari

Received: 4 April 2010 / Accepted: 6 September 2010 / Published online: 18 September 2010

Abstract A series of $LiM_{1x}M_{2y}Mn_{2-x-y}O_{3.8}F_{0.2}$ (M_1 = Cr, M_2 = V; x = y = 0.2) cathodes, viz., $LiMn_2O_{3.8}F_{0.2}$, $LiCr_{0.2}Mn_{1.8}O_{3.8}F_{0.2}$ and $LiCr_{0.2}V_{0.2}Mn_{1.6}O_{3.8}F_{0.2}$ along with native $LiMn_2O_4$ have been synthesized by Citric Acid assisted Modified (CAM) sol–gel method, with a view to understand the effect of synthesis methodology and the effect of dual category dopants, viz., anion and/or cation upon spinel cathodes individually. An acceptable capacity retention (94%) observed up to 50 cycles for native $LiMn_2O_4$ cathodes is attributed to the significance of CAM sol–gel method. Similarly, the encouraging charge–discharge results of $LiMn_2O_{3.8}F_{0.2}$ (130 mAh g^{-1}) and $LiCr_{0.2}Mn_{1.8}O_{3.8}F_{0.2}$ (142 mAh g^{-1}) cathodes revealed a possible augmentation in the reversible capacity behavior of the spinels upon F^- substitution at *32e* site and the simultaneous substitution of Cr^{3+} and F^- at *16d* and 32e sites respectively.

Keywords $LiMn_2O_4$ cathodes · Cation and anion doping · MAS ^{7}Li-NMR · Specific capacity · Lithium batteries

1 Introduction

$LiMn_2O_4$ with the $A[B_2]O_4$ spinel structure is popularly known for its ability to exhibit high electrode potential and specific capacity during the process of lithium extraction and reinsertion on the 4 V plateau [1]. However, the major limitation of $LiMn_2O_4$ as an electrode material is that the reversible 4 V capacity tends to fade upon electrochemical cycling, due to factors such as (i) Fracture of the particle surface due to local Jahn–Teller distortions at high rates of discharge [2] (ii) Dissolution of manganese from lithiated [3] and delithiated spinels [4], (iii) Electrolyte oxidation on the spinel surface [5], (iv) Cation mixing, or Li/Mn site exchange [6], (v) Loss of oxygen from the spinel [7] and (vi) Structural failure in the two-phase reaction region [8]. Therefore several attempts are being made to alleviate the aforesaid problems, which include the selection of compatible electrolytes, coating of the spinel particles with a chemically stable species, tuning of physical parameters such as phase purity, particle size, surface area, etc., by way of adopting optimized synthesis procedure, and partial substitution of suitable dopants for manganese/oxygen ions [9].

Among the various possibilities, partial substitution of certain divalent and trivalent metal cations for Mn^{3+} and the adoption of suitable synthesis methodology are widely studied and reported to enhance the electrochemical properties of $LiMn_2O_4$ spinels significantly [10]. Moreover, these two approaches are simple to adopt and practically viable in nature. On the other hand, oxygen deficiency which is common, especially at high sintering temperature [11] is also a source of distortion of the spinel, that can not be ignored while addressing the problem of unacceptable capacity fade of $LiMn_2O_4$ upon progressive cycling. Towards this direction, suppression of oxygen partial pressure, via., anion substitution, namely, fluorine for oxygen gains paramount importance for two reasons: (a) Anion (fluorine) substitution is less studied than cation substitution, thus stressing the need to have more understanding on the same. (b) Oxygen partial pressure problem directly hampers the lithium diffusion kinetics and reduces the deliverable capacity drastically, thus

N. Jayaprakash · N. Kalaiselvi (✉) · Gangulibabu · D. Bhuvaneswari
Central Electrochemical Research Institute, Karaikudi 630 006, India
e-mail: kalakanth2@yahoo.com

C. H. Doh
Korea Electro Technology Research Institute, Changwon 641 600, South Korea

requiring more attention to address this critical issue. As a result, effect of fluorine (anion) substitution for oxygen has been planned to study the combined effect of simultaneous substitution of an anion and cation(s) in the native $LiMn_2O_4$ spinel matrix.

Already literature is replete with the reports on the partial substitution of suitable metal dopants for Mn^{3+} that increases the co-valency [12] in the metal–oxygen bond and delays the onset of the Jahn–Teller distortion during discharge to enhance the electrochemical properties of the $LiMn_2O_4$ cathode [13]. However, limited reports are only available on the doping of anion site with florine [14–16] and the simultaneous substitution of an anion [for oxygen] and cation(s) [for Mn^{3+}]. Therefore, an attempt has been made through the present study to understand the combined effect of partial substitution of certain select category metal cations, viz., Cr^{3+} and/or V^{5+} for Mn^{3+} [cation substitution] along with the effect of F^- substitution for oxygen in the native $LiMn_2O_4$ spinel. Hence, a series of $LiMn_2O_4$ derived spinels, viz., $LiMn_2O_{3.8}F_{0.2}$, $LiCr_{0.2}Mn_{1.8}O_{3.8}F_{0.2}$ and $LiCr_{0.2}V_{0.2}Mn_{1.6}O_{3.8}F_{0.2}$ were synthesized and characterized further for their physical as well as electrochemical properties. Particularly, it is aimed to understand the effect of anion (F^-) substitution, combined anion–cation (F^- and Cr^{3+}) effect and the synergistic effect of anion and bi-cation substitutions (F^-, Cr^{3+} and V^{5+}) individually, which is the significance of the present investigation.

As mentioned earlier, identification and adoption of a suitable synthesis methodology with optimized synthesis parameters/conditions are reported to play a vital role in modifying both the physical as well as electrochemical properties of a cathode material [17]. In this connection, a simple and an easy-to-adopt one-pot synthesis methodology has been chosen to synthesize the title compounds. i.e., based on our earlier studies [17] Citric Acid assisted Modified (CAM) sol–gel method has been adopted to synthesize the series of $LiMn_2O_4$, $LiMn_2O_{3.8}F_{0.2}$, $LiCr_{0.2}Mn_{1.8}O_{3.8}F_{0.2}$ and $LiCr_{0.2}V_{0.2}Mn_{1.6}O_{3.8}F_{0.2}$ cathodes of the present study.

In short, the present study is bestowed with an explorative attempt to understand the possibility and the extent of enhancing the electrochemical properties of $LiMn_2O_4$ based cathodes through partial substitution of suitable dopants (for Mn^{3+} and O^{2-}) and the adoption of CAM sol–gel method.

2 Experimental

2.1 Synthesis procedure

The anionic and cationic substituted spinel phase $LiMn_2O_4$ active materials were synthesized by adopting Citric acid Assisted Modified sol–gel [CAM sol–gel] method, wherein the reaction proceeds in an acidic environment created by the addition of an organic acid. Stoichiometric proportions of high purity respective metal acetates viz., CH_3COOLi, $Mn(CH_3COO)_2{\cdot}4H_2O$, $Cr(NO_3)_3{\cdot}9H_2O$ [for doping Cr^{3+}] and NH_4VO_3 [for doping V^{5+}] (Sigma-Aldrich, India) and LiF [for doping F^-] were selected as precursors and citric acid was added as a complexing agent, followed by the addition of acryl amide and *N′N*-methylene bis acryl amide. Details pertaining to the CAM sol–gel synthesis approach, viz., role of various additives deployed in the synthesis methodology, precautionary measures to be adhered during the process of furnace calcinations, etc., are elaborated elsewhere [17].

2.2 Physical and electrochemical characterization

Phase characterization was done from the powder X-ray diffraction (XRD) patterns recorded on a Philips 1830 X-ray diffractometer using Ni filtered Cu–Kα radiation ($\lambda = 1.5406$ Å) in the 2θ range of 10°–80° at a scan rate of 0.04° s^{-1}. Surface morphology and the percentage composition of various elements/metals present in the synthesized active materials were investigated using Scanning Electron Microscopy (SEM) coupled with EDAX (Energy-dispersive X-ray analysis) results obtained from Jeol S-3000 H Scanning Electron Microscope. ^{7}Li NMR measurements were carried out with a Bruker MSL-400 spectrometer by employing a 5 mm Bruker VT-MAS probe operating at a ^{7}Li frequency of 14 MHz. For the current study, a one-pulse sequence was used with a pulse length of 3 μs along with a recycle delay of 500 ms for about 100,000 scans. Room temperature electrochemical studies such as cyclic voltammetry (CV) and charge–discharge measurements were performed using an Autolab Electrochemical Workstation and MACCOR charge–discharge cycle life tester, respectively. In this connection, crimp sealed 2016 coin cells containing lithium metal anode, synthesized $LiMn_2O_4$ derived cathode material and a non-aqueous electrolyte containing 1 M $LiPF_6$ salt dissolved in 1:1 v/v ethylene carbonate (EC) and dimethyl carbonate (DMC) solvent were deployed, wherein polypropylene separator was used.

2.3 Electrode preparation and cell assembly

The process of electrode preparation and the coin cell fabrication in an Argon-filled Glove box are mentioned in our earlier reports [18].

3 Results and discussion

3.1 Structural results-PXRD studies

The X-ray diffraction results of series of $LiMn_2O_4$ compounds containing F^- as the anionic substitute and Cr^{3+}

and V^{5+} as the cation substitutes are shown in Fig. 1. The miller indices *(hkl)* of all the peaks corresponding to the parent $LiMn_2O_4$ and its doped derivatives are indexed as per the JCPDS file No: 35-0782, that corroborates the existence of a cubic spinel structure with *Fd*3 *m* space group. Therefore, it is presumed that Li^+ ions occupy the *8a* tetrahedral sites, Cr^{3+}, V^{5+} and Mn^{4+} ions are located arbitrarily at the octahedral *16d* sites, and O^{2-} and F^- ions are located at the 32*e* sites. The slight variation in the lattice parameter values (Table 1) of the substituted $LiMn_2O_4$ from the un doped parent spinel is an indication that the dopants viz., Cr^3, V^{5+}, F^- are successfully incorporated into the native $LiMn_2O_4$ matrix. Further, the deployment of duly controlled optimum synthesis temperature (800 °C) with an intermittent grinding has resulted in the formation of highly crystallized products, as obvious from the PXRD peaks with high intensity (Fig. 1). Similarly, the presence of undesirable impurities (viz., Li_2O, Mn_2O_3, $Li_2Mn_3O_4$) and the probable lithium loss at high temperature synthesis process have successfully been excluded by the adoption of CAM sol–gel method, which is noteworthy.

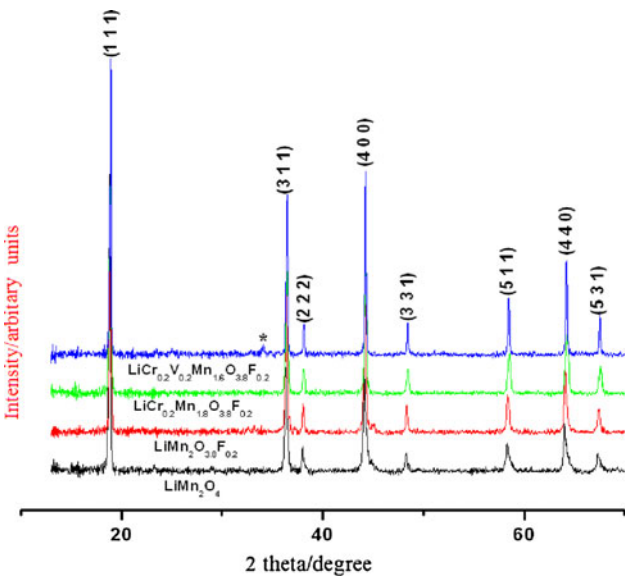

Fig. 1 X-ray diffraction pattern of $LiM_{1x}M_{2y}Mn_{2-x-y}O_{3.8}F_{0.2}$ (M_1 = Cr, M_2 = V; x = y = 0.2) cathodes

Table 1 Physical parameters of the $LiM_{1x}M_{2y}Mn_{2-x-y}O_{3.8}F_{0.2}$ (M_1 = Cr, M_2 = V; x = y = 0.2) cathodes (derived from PXRD)

Compound	Lattice constant a (Å)	Cell volume a^3(Å)
$LiMn_2O_4$	8.145	540.34
$LiMn_2O_{3.8}F_{0.2}$	8.101	531.63
$LiCr_{0.2}Mn_{1.8}O_{3.8}F_{0.2}$	8.120	535.38
$LiV_{0.2}Cr_{0.2}Mn_{1.6}O_{3.8}F_{0.2}$	8.105	532.42

3.2 Morphological results-SEM analysis

The surface morphology of synthesized compounds viz., $LiMn_2O_4$, $LiMn_2O_{3.8}F_{0.2}$, $LiCr_{0.2}Mn_{1.8}O_{3.8}F_{0.2}$ and $LiCr_{0.2}V_{0.2}Mn_{1.6}O_{3.8}F_{0.2}$, sintered at 800 °C are furnished in Fig. 2a–d. Presence of evenly distributed spherical grains encompassing a large number of size reduced particles is observed for the parent $LiMn_2O_4$ (Fig. 2a). Similarly, the anion (F^-) and cations (Cr^{3+} and/or V^{5+}) substituted derivatives of $LiMn_2O_4$ also exhibited finer particles with well defined grain boundary, as obvious from the micrographs displayed in Fig. 2b–d. Generally, sintering the precursor above 700 °C makes the particles to fuse together partially to form large porous agglomerates, regardless of post grinding treatment after the decomposition step [19]. However, neither an increased particle size nor particle agglomeration are found in the present case, which is the significance of CAM sol–gel method.

Further, the stoichiometry of the synthesized cathode materials were verified using EDAX analysis (Fig. 3a–d). The percentage of the individual elements, except Li has been confirmed, since it is not practically possible to calculate the percentage of lithium present in the synthesized compound by applying EDAX.

3.3 ^{7}Li MAS-NMR spectral studies

Lithium NMR plays an important role among the methods that are generally deployed to study battery materials, as it probes the local environments surrounding the lithium ions, which are directly involved in the electrochemical processes [20]. Basically, $LiMn_2O_4$ spinel cathode is a mixedvalent compound containing both Mn^{3+} and Mn^{4+} ions and a hopping semiconductor, wherein hopping occurs between the e.g., orbitals of the manganese ions [21]. Since this hopping timescale is faster than the NMR time scale ($\approx 10^{-5}$ s), the lithium spins encounters an average manganese oxidation state of 3.5 (i.e., $Mn^{3.5+}$ ions), and thus there is only one magnetically unequal lithium site (8*a* site) in the $LiMn_2O_4$ spinel [21].

The ^{7}Li MAS NMR spectra of both the undoped and doped $LiMn_2O_4$ samples synthesized in air at 800 °C are shown in Fig. 4a–d. Herein, the spectral pattern witnessed large shifts from the shift position typically obtained for diamagnetic solids at around 0 ppm along with larger spinning sideband manifolds. Among the spinels chosen for the study, ($LiMn_2O_4$, $LiMn_2O_{3.8}F_{0.2}$, $LiMn_{1.8}Cr_{0.2}O_{3.8}F_{0.2}$ and $LiMn_{1.6}Cr_{0.2}V_{0.2}O_{3.8}F_{0.2}$), presence of two intense resonances around 515–536 and 612–620 ppm is seen for all the compounds, with an exception of

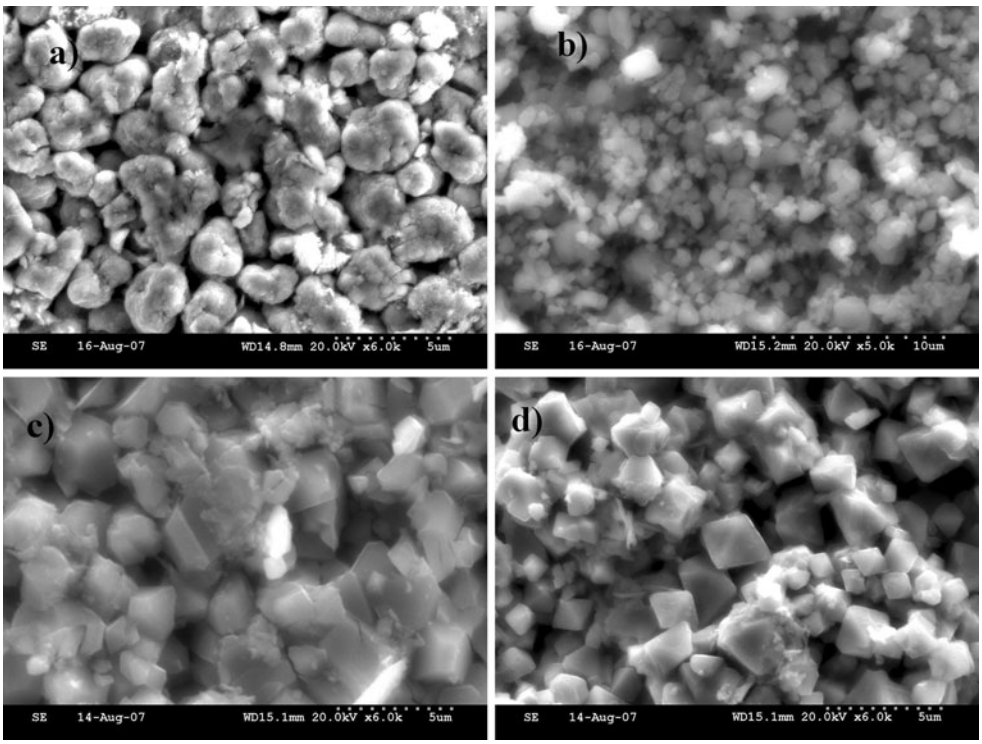

Fig. 2 SEM images of **a** $LiMn_2O_4$ **b** $LiMn_2O_{3.8}F_{0.2}$ **c** $LiCr_{0.2}Mn_{1.8}O_{3.8}F_{0.2}$ and **d** $LiCr_{0.2}V_{0.2}Mn_{1.6}O_{3.8}F_{0.2}$

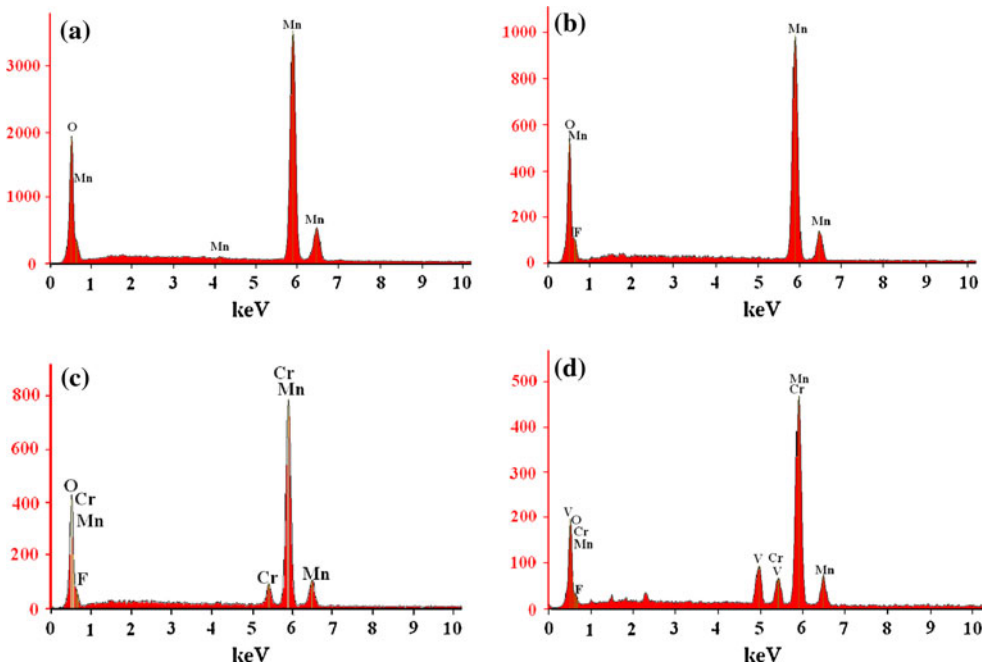

Fig. 3 EDAX spectra obtained from an area scan micrograph of **a** $LiMn_2O_4$ **b** $LiMn_2O_{3.8}F_{0.2}$ **c** $LiCr_{0.2}Mn_{1.8}O_{3.8}F_{0.2}$ and **d** $LiCr_{0.2}V_{0.2}Mn_{1.6}O_{3.8}F_{0.2}$

$LiMn_{1.6}Cr_{0.2}V_{0.2}O_{3.8}F_{0.2}$, wherein an additional resonance at 0 ppm is observed.

The major resonance at ~520 ppm of $LiMn_2O_4$ (Fig. 4a) is assigned to a lithium cation in the normal tetrahedral *8a* site of the spinel structure, based on the reports of Morgan et al. [22], wherein a single isotropic resonance at 520 ppm alone is observed for $LiMn_2O_4$. Similarly, the second intense resonance at 620 ppm may be assigned to lithium cations surrounding the defects, consisting of *16d* manganese vacancies [23]. In other words, the peak at ~620 ppm is attributed to the lithium near *16d* manganese vacancies, which is in agreement with the reports of

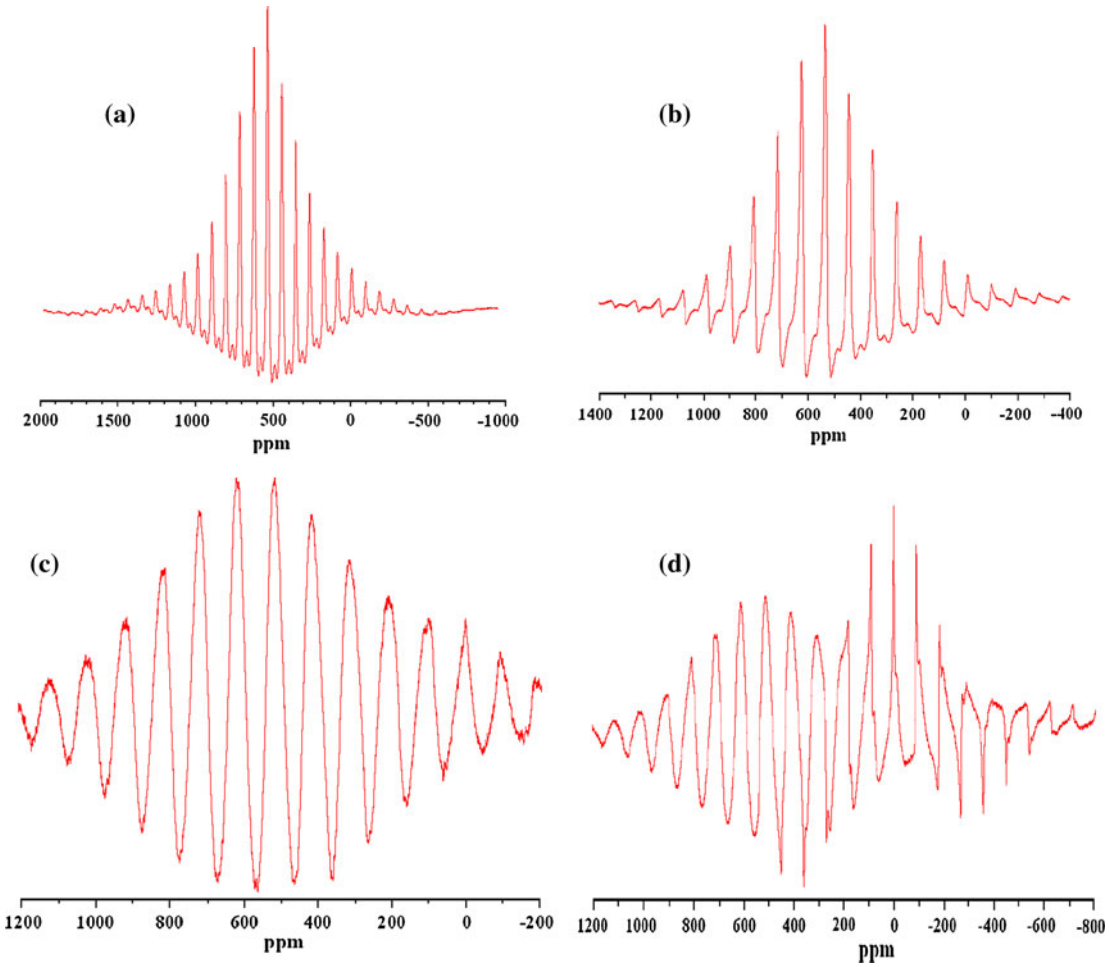

Fig. 4 ^{7}Li MAS NMR spectra of **a** $LiMn_2O_4$ **b** $LiMn_2O_{3.8}F_{0.2}$ **c** $LiCr_{0.2}Mn_{1.8}O_{3.8}F_{0.2}$ and **d** $LiCr_{0.2}V_{0.2}Mn_{1.6}O_{3.8}F_{0.2}$

Thackeray et al. [24]. This explanation holds good for $LiMn_2O_{3.8}F_{0.2}$ (Fig. 4b) also, which has displayed a closer similarity with the parent $LiMn_2O_4$, except for the appearance of a few extra spinning sidebands. The presence of spinning side bands epitomizes the fact that the anionic substitution of fluorine takes place only at *32e* site, by way of reducing the oxygen partial pressure, without affecting the lithium local environment. Likewise, the similarity in the ^{7}Li NMR pattern of $LiCr_{0.2}Mn_{1.8}O_{3.8}F_{0.2}$ (Fig. 4c) with the parent spinel is in favor of the fact that the partial substitution of Cr^{3+} (for Mn^{3+}) has taken place in the *16d* site successfully without affecting the lithium local environment.

On the other hand, it is quite interesting to note that the ^{7}Li NMR spectral pattern of $LiCr_{0.2}V_{0.2}Mn_{1.6}O_{3.8}F_{0.2}$ compound (Fig. 4d) consists of three resonance peaks at 615, 515 and 0 ppm. As discussed earlier, the peaks at 515 and 615 ppm are attributed to the lithium ions present in the normal tetrahedral (*8a*) site and the near Li defects which might consist of *16d* Mn vacancies [23]. According to earlier reports, the existence of additional resonance at 0 ppm may generally be correlated with the presence of trace amount lithium fluoride [25]. However, the possible presence of unreacted LiF, deployed to impart fluorine doping in $LiMn_2O_4$ spinel structure is not applicable to the present case for two reasons: (a) No excess amount of LiF has been used in the synthesis process: rather, an exact and stoichiometric proportion of LiF has been treated with the rest of the precursor mix followed by the carefully monitored calcination sequence and (b) PXRD results clearly authenticate the absence of trace quantities of excess or unreacted LiF in the final product.

Alternatively, the presence of an additional resonance at 0 ppm may be understood as follows: actually, among the two transition metal dopants viz. Cr^{3+} and V^{5+}, chromium will occupy the targeted *16d* site [26], whereas vanadium has the possibility of occupying either *16d* or *8a* site [27]. As a result, part of the lithium replaced by vanadium occupying the 8a position is believed to cause the additional resonance at 0 ppm.

Similarly, the resonance at 0 ppm of $LiCr_{0.2}V_{0.2}Mn_{1.6}O_{3.8}F_{0.2}$ may be discussed from another angle also.

i.e., literature is replete with certain reports that penta valent metal dopants tend to form stable lithium compounds such as $LiMO_3$, etc., instead of phase pure spinel-type lithium metal (V) manganese oxide [28]. Based on this, the additional peak at 0 ppm may be attributed to the possible presence of trace amount of Li–V–O impurity and the same is substantiated further from the poor electrochemical characteristics of $LiCr_{0.2}V_{0.2}Mn_{1.6}O_{3.8}F_{0.2}$ compound (discussed below). Towards this direction, the presence of a significant peak at $2\theta = 35°$ in the XRD pattern of $LiCr_{0.2}V_{0.2}Mn_{1.6}O_{3.8}F_{0.2}$ compound (marked as * in Fig. 1) may also be revisited and correlated to the possible presence of Li–V–O related impurities.

Among the two possibilities discussed for the occurrence of 0 ppm resonance, the former explanation concerned with the removal of Li by V in *8a* position has no supporting evidence in the current study, whereas the later one for the formation of Li–V–O impurity is justified from XRD (Fig. 1) as well as from the charge–discharge results (discussed below) of the $LiCr_{0.2}V_{0.2}Mn_{1.6}O_{3.8}F_{0.2}$ compound. Hence, it is derived that the additional resonance at 0 ppm of $LiCr_{0.2}V_{0.2}Mn_{1.6}O_{3.8}F_{0.2}$ compound is due to the presence of trace amount of Li–V–O based impurity. Further, based on the intriguing results obtained for $LiCr_{0.2}V_{0.2}Mn_{1.6}O_{3.8}F_{0.2}$ compound, a detailed investigation on the same to exploit $LiCr_{0.2}V_{0.2}Mn_{1.6}O_{3.8}F_{0.2}$ cathode for lithium battery applications is planned for our future study.

3.4 Electrochemical characterization

3.4.1 Cyclic voltammetry studies

The electrochemical stability of the synthesized $LiMn_2O_4$, $LiMn_2O_{3.8}F_{0.2}$, $LiMn_{1.8}Cr_{0.2}O_{3.8}F_{0.2}$ and $LiMn_{1.6}Cr_{0.2}V_{0.2}O_{3.8}F_{0.2}$ cathodes were investigated using Cyclic Voltammetry. Figure 5a–d show the representative slow scan cyclic voltammograms of the synthesized compounds recorded at room temperature, under a sweep rate of 0.5 mV s^{-1}. Herein, the potential window is fixed between 2.0 and 4.5 V vs. Li/Li^+, with a view to examine the stability of the synthesized cathode materials upon over discharge (up to 2.0 V region) condition. Because, over discharge (below 3.0 V) in general may lead to serious capacity fading due to Jahn–Teller distortion, dissolution of manganese, etc., [29]. Hence, it is planned through the present study to investigate upon the possibility of maintenance of minimized Jahn–Teller distortion even on over discharge (up to 2.0 V) condition, by way of introducing suitable dopants and by adopting a suitable CAM sol–gel synthesis methodology.

The observed CV results of all the spinel cathodes are displayed in Fig. 5a–d. It is interesting to note that all the four cathodes have exhibited two pairs of well resolved peaks at 4.12, 3.89 V and 4.24, 4.09 V, indicating a two-step reversible intercalation/deintercalation of lithium between $LiMn_2O_4$ and λ-MnO_2. This observation is in good agreement with the two flat plateaus in the discharge curves shown in Fig. 6a–d, thus substantiating the normal process of lithium intercalation/de-intercalation in $LiMn_2O_4$ related spinels [30].

Besides the presence of two pairs of peaks for the 4 V process, there appeared a pair of distinguished 3 V region peaks, viz., 3.20 V on charge and 2.73 V on discharge as evident from Fig. 5a–d. Such a peak pair in 3 V region corresponds to the intercalation of lithium into $LiMn_2O_4$, wherein the average oxidation state of manganese is reduced from 3.5 to 3, along with a possible change of structure from cubic to tetragonal [31]. Similarly, an extra anodic peak at 3.85 V appears from second cycle onwards, due to the extraction of residual lithium from the octahedral sites. It is noteworthy that the peak at 3.85 V is neither observed in the typical CV of $LiMn_2O_4$ and related cathodes, cycled between 3.0 and 4.5 V [32] nor in the first CV of the present study with the over discharge potential window (2.0–4.5 V). Rather, the 3.85 V peak is found to appear only from the second charging, especially after the discharge of $LiMn_2O_4$ electrode down to 2.0 V. Hence, it is understood that the appearance of such 3.85 V peak is due to the occurrence of possible structural distortion in the 3 V region that leads to the partial residues of lithium in octahedral sites which are difficult to be extracted at 3.20 V itself. Further, the consistent presence of cathodic peak at 2.73 V substantiates the fact that the minimized John–Teller distortion through partial substitution of anion and/or cation is maintained even during over discharge, which is the highlight of the present study.

The current–voltage curves displayed in Fig. 5a clearly exhibits the excellent reproducibility of anodic and cathodic peaks, especially upon successive cycles. Further, significant enhancement in the peak current is also observed for $LiMn_2O_{3.8}F_{0.2}$ and $LiMn_{1.8}Cr_{0.2}O_{3.8}F_{0.2}$ cathodes (Fig. 5b and c), thus arbitrates the augmentation of excellent reversibility of insertion/extraction of Li ions. Hence, it is demonstrated that Jahn–Teller distortion is reduced via. partial substitution of select category Cr^{3+} and F^- dopants in *16d* and *32e* sites, respectively. From Fig. 5c–d, it is understood that the substitution of Cr^{3+} to the spinel phase $LiMn_2O_4$ has caused the merger of two pairs of redox peaks at 4.12, 3.89 V and 4.24, 4.09 V into one, which is in agreement with the reported results of Fu etal. [33]. On the other hand, the CV of anion and bi-cation substituted $LiMn_{1.6}Cr_{0.2}V_{0.2}O_{3.8}F_{0.2}$ cathode (Fig. 5d) displayed a poor reversibility accompanied by reduced peak current, which is attributed to the formation of stable

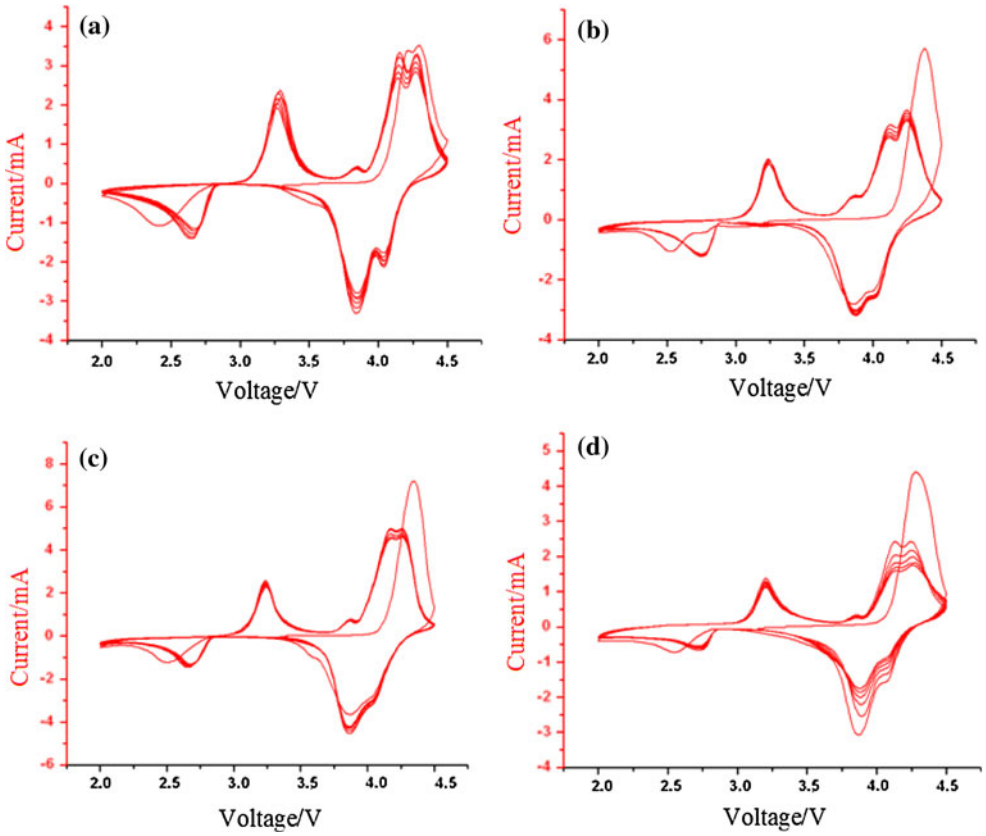

Fig. 5 Cyclic Voltammogram of **a** $LiMn_2O_4$ **b** $LiMn_2O_{3.8}F_{0.2}$ **c** $LiCr_{0.2}Mn_{1.8}O_{3.8}F_{0.2}$ and **d** $LiCr_{0.2}V_{0.2}Mn_{1.6}O_{3.8}F_{0.2}$ recorded at a scan rate of 0.5 mV/s

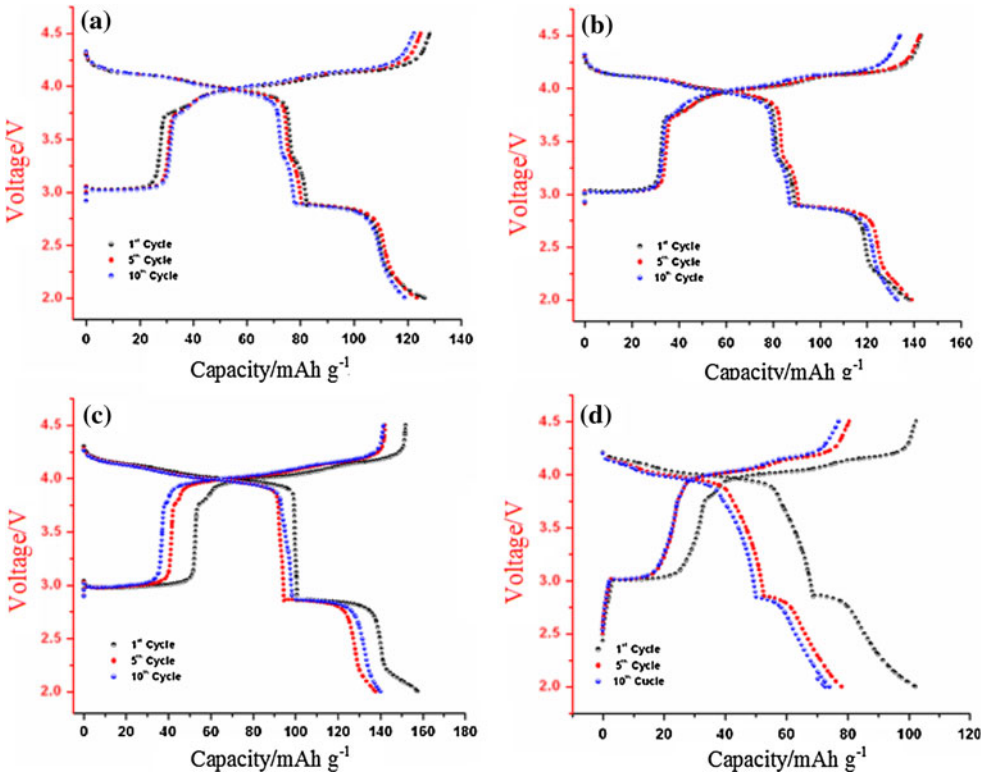

Fig. 6 Voltage versus capacity behavior of **a** $LiMn_2O_4$ **b** $LiMn_2O_{3.8}F_{0.2}$ **c** $LiCr_{0.2}Mn_{1.8}O_{3.8}F_{0.2}$ and **d** $LiCr_{0.2}V_{0.2}Mn_{1.6}O_{3.8}F_{0.2}$

lithium vanadium (Li–V–O) compound, as discussed in ^{7}Li MAS NMR studies.

Hence, it is derived from both the CV and ^{7}Li MAS NMR studies that among the chosen category dopants, Cr^{3+} and F^{-} qualify themselves, respectively, as suitable cation and anion dopants, whereas V is not found to be an advantageous dopant, since it has reduced the CV peak current value, despite the presence of Cr^{3+} dopant in $LiMn_{1.6}Cr_{0.2}V_{0.2}O_{3.8}F_{0.2}$ cathode.

3.4.2 Electrochemical charge–discharge studies

The discharge curves of the parent and doped $LiMn_2O_4$ compounds were measured at a current density of 0.2 mA and in the potential window of 2.0–4.5 V, to exemplify the effect of over discharge and to demonstrate the structural stability of synthesized cathodes upon the same. The observed specific capacity values as a function of cycle life behavior are furnished in Table 2.

Figure 6 shows the charge–discharge behavior of $Li/LiMn_2O_4$, $Li/LiMn_2O_{3.8}F_{0.2}$, $Li/LiCr_{0.2}Mn_{1.8}O_{3.8}F_{0.2}$ and $Li/LiV_{0.2}Cr_{0.2}Mn_{1.6}O_{3.8}F_{0.2}$ half-cells. As obvious form the figure, all the $LiMn_2O_4$ based cathodes have exhibited 2 voltage plateaus at about 4.0 and 4.1 V, thus substantiating the formation of well defined spinel structure. Further, it is understood that the appearance of two plateaus correspond to the insertion and extraction of lithium ions in two stages [34]. In other words, the plateau at 4.0 V arises due to the removal of lithium ions from half of the tetrahedral sites and the second plateau at 4.1 V corresponds to the removal of lithium ions from the other tetrahedral sites [35].

Further, it is very interesting to note that the initial irreversible capacity loss is minimized via., anion as well as cation(s) substitution into the native $LiMn_2O_4$ structure, as evident from Figs. 6a–d and 7. Actually, both the undoped and F^{-} doped $LiMn_2O_4$ cathodes exhibit high initial specific capacity (129 and 143 mAh g^{-1}, respectively) values with an enhanced structural stability and lesser capacity fade (<10%) upon cycling. Particularly, the parent $LiMn_2O_4$, popularly known for its unacceptable capacity fade [36] upon over discharge is found to exhibit better capacity retention (94%), up to 50 cycles (Fig. 6a–b), which is attributed to the significant outcome of CAM sol–gel methodology. Similarly, $LiMn_2O_{3.8}F_{0.2}$ cathode has exhibited a steady-state capacity of ~130 mAh g^{-1} throughout the process of extended cycling (50 cycles), which is an indication that the synergistic effect of anion (F^{-}) substitution and the adoption of CAM sol–gel method have resulted in the remarkable suppression of oxygen partial pressure problem, despite the high temperature sintering at 800 °C.

Interestingly, $LiCr_{0.2}Mn_{1.8}O_{3.8}F_{0.2}$ cathode (Fig. 6c) has exhibited the highest initial discharge capacity (159 mAh g^{-1}), and more interestingly, a near zero-strain electrode behavior with 142 mAh g^{-1} capacity and <1% capacity fade (Fig. 7) has been achieved by the same from third cycle onwards. Despite the literature reports that deal with the possibility of over discharge-induced manganese dissolution and structural deterioration [37], for Cr^{3+} dopants, the present study has completely overlooked such hampering issues and exhibited the highest capacity behavior mainly due to Cr^{3+} substitution.

In short, the observed high specific capacity values (130–155 mAh g^{-1}) and the well controlled capacity fade behavior of $LiMn_2O_4$ and the duly (F^{-} and/or Cr^{3+}) substituted $LiMn_2O_4$ cathodes of the present investigation are superior than many of the earlier reports on $LiMn_2O_4$ [38] related spinel cathodes of lithium batteries. Such an improved electrochemical characteristic may be attributed to the synergistic effect of synthesis methodology and the incorporation of suitable dopants to the native $LiMn_2O_4$ structure.

On the other hand, potential vs. capacity plot of the bi cation (Cr^{3+} and V^{5+}) and fluorine doped $LiMn_2O_4$ cathode, viz., $LiCr_{0.2}V_{0.2}Mn_{1.6}O_{3.8}F_{0.2}$ displayed a reduced initial capacity (105 mAh g^{-1}) and an increased irreversible capacity loss (>40%), compared to the rest of

Table 2 Charge–discharge characteristics of $LiM_{1x}M_{2y}Mn_{2-x-y}O_{3.8}F_{0.2}$ (M_1 = Cr, M_2 = V; x = y = 0.2) cathodes

Compound	Discharge capacity (mAh g^{-1})	
	Qdc_1	Qdc_{50}
$LiMn_2O_4$	128.3	121.6
$LiMn_2O_{3.8}F_{0.2}$	142.7	129.8
$LiCr_{0.2}Mn_{1.8}O_{3.8}F_{0.2}$	158.8	141.7
$LiV_{0.2}Cr_{0.2}Mn_{1.6}O_{3.8}F_{0.2}$	105.0	62.5

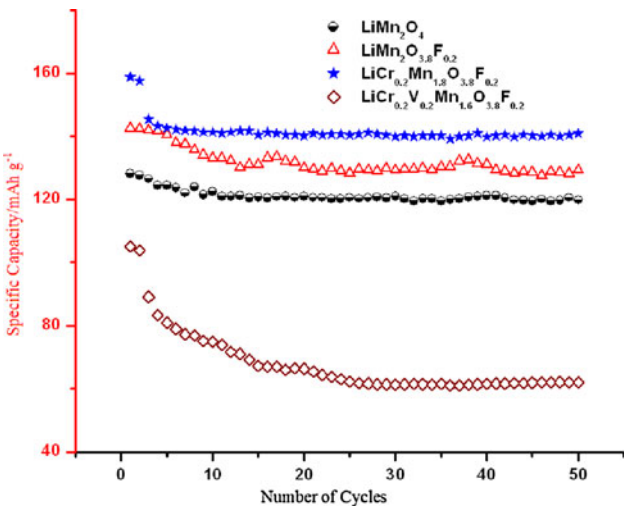

Fig. 7 Capacity versus cycle life characteristics

the cathodes (Fig. 6d). This may be attributed to the presence of trace amount of vanadium based impurity produced by the penta valent vanadium dopant, as discussed through ^{7}Li MAS NMR and CV studies.

Figure 7a–d represents the cycle life vs. capacity plot of $LiMn_2O_4$, $LiMn_2O_{3.8}F_{0.2}$, $LiCr_{0.2}Mn_{1.8}O_{3.8}F_{0.2}$ and $LiV_{0.2}Cr_{0.2}Mn_{1.6}O_{3.8}F_{0.2}$ cathodes, respectively. It is interesting to note that the introduction of fluorine to the parent $LiMn_2O_4$ has effectively increased the reversible capacity from 123 to130 mAh g^{-1}. In addition, the reversible capacity due to the simultaneous substitution of Cr^{3+} and F^{-} has enhanced and maintained the same further to an extent of 142 mAh g^{-1}, even up to 50 cycles. The reason for the significantly improved capacity value of $LiCr_{0.2}Mn_{1.8}O_{3.8}F_{0.2}$ is due to the combined effect of synthesis methodology and the Cr^{3+} and F^{-} dopants [39, 40], via. enhanced stability of the octahedral sites in the spinel skeleton (Cr^{3+}) and the suppressed oxygen partial pressure (F^{-}). Further, it is believed that the partial substitution of Mn^{3+} with Cr^{3+} decreases the unit cell volume and the corresponding decrease in Mn^{3+} concentration would reduce the Jahn–Teller distortion to the extent that the structural integrity and electrochemical stability of $LiCr_{0.2}Mn_{1.8}O_{3.8}F_{0.2}$ are higher than both the un doped $LiMn_2O_4$ and $LiMn_2O_{3.8}F_{0.2}$ cathodes (Figs. 6c and 7c).

On the contrary, the capacity fade per cycle is large for $LiCr_{0.2}V_{0.2}Mn_{1.6}O_{3.8}F_{0.2}$, (0.227% per cycle) which may be attributed to a possible volume expansion that occurs, especially upon over discharge that results in the change of cubic to tetragonally distorted structure. Hence, it is understood from the study that among the four cathodes synthesized, $LiMn_2O_4$ and $LiMn_2O_{3.8}F_{0.2}$ cathodes have demonstrated excellent reversible capacity. Similarly, $LiCr_{0.2}Mn_{1.8}O_{3.8}F_{0.2}$ cathode has exhibited the highest specific capacity with excellent capacity retention, compared to that of $LiV_{0.2}Cr_{0.2}Mn_{1.6}O_{3.6}F_{0.2}$ cathode.

4 Conclusion

By adopting CAM sol–gel method, series of spinel cathodes with the general formula $LiM_{1x}M_{2y}Mn_{2-x-y}O_{3.8}F_{0.2}$ (M_1 = Cr, M_2 = V; x = y = 0.2) were synthesized with a view to understand the effect and extent of doping and synthesis methodology in enhancing the electrochemical properties of native $LiMn_2O_4$. The effect of CAM sol–gel synthesis methodology has been realized in terms of desirable physical as well as enhanced electrochemical properties, exhibited by the synthesized cathode materials. More specifically, the un doped $LiMn_2O_4$ has exhibited an extraordinary capacity retention behavior (94%), due to the adoption of CAM sol–gel method. Similarly, the effect of fluorine doping in the parent $LiMn_2O_4$ has increased the capacity of $LiMn_2O_{3.8}F_{0.2}$ cathode (130 mAh g^{-1}) and the simultaneous doping of Cr^{3+} and F^{-} has resulted in the enhancement of the overall reversible capacity (142 mAh g^{-1}) and capacity retention (99%) of $LiCr_{0.2}Mn_{1.8}O_{3.8}F_{0.2}$ compared to the other cathode viz., $LiV_{0.2}Cr_{0.2}Mn_{1.6}O_{3.6}F_{0.2}$. In other words, combined anion and bi-cation substitution has failed to improve the electrochemical properties of native $LiMn_2O_4$, due to the unavoidable presence of Li–V–O impurities that has resulted due to the V^{5+} dopant of $LiV_{0.2}Cr_{0.2}Mn_{1.6}O_{3.6}F_{0.2}$.

However, the size reduced particles of all the $LiMn_2O_4$ derived doped spinels have facilitated the lithium diffusion into and out of the crystals and thereby rendered the capacity retention by weakening of Jahn–Teller distortion. Similarly, the minimized Jahn–Teller distortion due to the process of doping was found to get maintained even below 3.0 V range, that has prevented the over discharge induced rapid capacity fade, with an exception of $LiV_{0.2}Cr_{0.2}Mn_{1.6}O_{3.6}F_{0.2}$. Among the cathodes studied, $LiCr_{0.2}Mn_{1.8}O_{3.6}F_{0.2}$ is recommended as the potential candidate, as it possesses the highest reversible capacity and near zero-strain electrode behavior.

Acknowledgments The authors are thankful to the Department of Science and Technology (DST), New Delhi for financial support to carry out this work.

References

1. Thackeray MM, David WIF, Bruce PG, Goodenough JB (1983) Mater Res Bull 18:461
2. Thackeray MM, Shao-Horn Y, Kahaian AJ, Kepler KD, Skinner E, Vaughey JT, Hackney SA (1998) Electrochem Solid-State Lett 1:7
3. Hunter JC (1981) J Solid State Chem 39:142
4. Wen SJ, Richardson TJ, Ma L, Striebel KA, Ross PN, Cairns EJ (1996) J Electrochem Soc 143:L136
5. Guyomard D, Tarascon JM (1994) Solid State Ion 69:222
6. Tarascon JM, McKinnon WR, Coowar F, Bowmer TN, Amatucci G, Guyomard D (1994) J Electrochem Soc 141:1421
7. Xia Y, Zhou Y, Yoshio M (1997) J Electrochem Soc 144:2593
8. Lee JH, Hong JK, Jang DH, Sun YK, Oh SM (2001) J Power Sources 89:7
9. Hyung-Wook Ha, Yun NanJi, Kim Keon (2007) Electrochim Acta 52:3236
10. Julien C, Ziolkiewicz S, Lemal M, Massot M (2001) J Mater Chem 11:1837
11. Xu XX, Yang J, Wang YQ, Nuli YN, Wang JL (2007) J Power Sources 174:1113
12. Hasegawa A, Yoshizawa K, Yamabe T (2000) J Electrochem Soc 147:4052
13. Horne CR (2000) PhD Thesis, University of California, Berkeley, CA
14. Du G, NuLi Y, Yang J, Wang J (2008) Mater Res Bull 43:3607
15. Matsumoto K, Fukutsuka T, Okumura T, Uchimoto Y, Amezawa K, Inaba M, Tasaka A (2009) J Power Sources 189:599
16. He Y-S, Pei L, Liao X-Z, Ma Z-F (2007) J Fluorine Chem 128:139

17. Jayaprakash N, Sathiyanarayanan K, Kalaiselvi N (2007) Electrochim Acta 52:2453
18. Kalaiselvi N, Doh C-H, Park C-W, Moon S-I, Yun M-S (2004) Electrochem Commun 6:1110
19. Jayaprakash N, Kalaiselvi N (2007) Electrochem Commun 9:620
20. Grey CP, Lee YJ (2003) Solid State Sci 5:883
21. Grey CP, Greenbaum SG (2002) MRS Bull 27:613
22. Morgan KR, Collier S, Burns G, Ooi K (1994) J Chem Soc Chem Commun 1719
23. Lee YJ, Wang F, Grey CP (1998) J Am Chem Soc 120:12601
24. Thackeray MM, de Kock A, David WIF (1993) Mater Res Bull 28:1041
25. Oka H, Kasahara S, Okada T, Iwata E, Okada M, Shoji T, Ohki H, Okuda T (2001) Solid State Ion 144:19
26. Tucker MC, Kroeck L, Reimer JA, Cairns EJ (2002) J Electrochem Soc 149:A1409
27. Kalyani P, Kalaiselvi N, Renganathan NG (2005) Mater Chem Phys 90:196
28. Chitrakar R, Kanoh H, Makita Y, Miyai Y, Ooi K (2000) J Mater Chem 10:2325
29. Tang SB, Lai MO, Lu L (2007) J Power Sources 164:372
30. Striebel KA, Deng CZ, Wen SJ, Cairns EJ (1996) J Electrochem Soc 143:1821
31. Rougier A, Striebel KA, Wen SJ, Cairns EJ (1998) J Electrochem Soc 145:2975
32. Tang SB, Lai MO, Lu L (2006) Electrochim Acta 52:1161
33. Fu YP, Su YH, Wu SH, Lin CH (2006) J Alloys Compd 426:228
34. Xia Y, Yoshio M (1996) J Electrochem Soc 143:825
35. He B, Zhou WJ, Liang YY, Bao SJ, Li HL (2006) J Colloid Interface Sci 300:633
36. Kalyani P, Kalaiselvi N, Muniyandi N (2002) J Power Sources 111:232
37. Chiu KF, Lin HC, Lin KM, Chen CC (2006) J Electrochem Soc 153:92
38. Nieto S, Majumder SB, Katiyar RS (2004) J Power Sources 136:88
39. Guohua L, Ikuta H, Uchida T, Wakihara M (1996) J Electrochem Soc 143:178
40. Kim JS, Vaughey JT, Johnson CS, Thackeray MM (2003) J Electrochem Soc 150:A1498